IEEE Access
Multidisciplinary ⋮ Rapid Review ⋮ Open Access Journal

Received January 19, 2022, accepted February 15, 2022, date of publication February 28, 2022, date of current version March 16, 2022.

Digital Object Identifier 10.1109/ACCESS.2022.3155449

Neural Network-Based Identification of a PSA Process for Production and Purification of Bioethanol

ERASMO MISAEL RENTERÍA-VARGAS[1], CARLOS JESÚS ZÚÑIGA AGUILAR[1], JESSE YOE RUMBO MORALES[1], (Member, IEEE), FELIPE DE JESÚS SORCIA VÁZQUEZ[1], MIGUEL DE-LA-TORRE[1], (Senior Member, IEEE), JOSÉ ANTONIO CERVANTES[1], ESTELA SARMIENTO BUSTOS[2], AND MANUELA CALIXTO RODRÍGUEZ[2]

[1]Computer Science and Engineering Department, University of Guadalajara, Ameca, Guadalajara 46600, Mexico
[2]Academic Division of Industrial Mechanics, Emiliano Zapata Technological University of the State of Morelos, Emiliano Zapata, Morelos 62760, Mexico

Corresponding author: Jesse Yoe Rumbo Morales (jesse.rumbo@academicos.udg.mx)

ABSTRACT The pressure swing adsorption (PSA) process, is a novel method for the purification and production of bioethanol. A highly non-linear rigorous model is implemented to simulate the cyclic dynamics of PSA, achieving purity of 99% wt of ethanol, which meets international standards to be used as fuel. The contribution of this work focuses on obtaining an identified model capable of capturing the important dynamics of the PSA process (with a fit above of 90%) and to be used for controller design purposes, since it is very complicated to design control in highly nonlinear models that are represented with partial differential equations (PDE). For proof of concept, a comparison between Hammersetein-Wienner and Artificial Neural-Networks showed the relevance of the proposed method, using the same input and output signals. Both identified models capture the important dynamics of the rigorous PSA model.

INDEX TERMS Artificial neural-networks, system identification, ethanol dehydration, pressure swing adsorption.

I. INTRODUCTION

Bioethanol is an alternative fuel that can be used in ignition engines and bivalent engines as a fuel or oxygen additive: E100 (100 % bioethanol) requires its own combustion technology; E85 (85 % bioethanol + 15 % gasoline) is used in the so-called FlexiFuel vehicles; the E5 (5 % bioethanol + 95 % gasoline) does not require modification of the vehicles. For its use to be possible, bioethanol needs to be free of water (it is then known as dehydrated ethanol). There are several alternatives to produce bioethanol, these are extractive distillation with salts, azeotropic distillation, vacuum distillation, pervaporation, and adsorption with molecular sieves. Currently, processes with molecular sieves have displaced certain technologies (azeotropic and extractive distillation with salts), since they have lower energy and equipment costs [1]. Another advantage of this process is obtaining purities of 99% ethanol compared to pervaporation processes that manage to reach purities close to 97% of ethanol. So that pervaporation processes achieve purity of 99% of ethanol, they need external equipment that involves other purification steps. To purify ethanol and achieve the properties of fuel ethanol, the adsorption process with molecular sieves has been used using the PSA method [1]–[7]. The highly non-linear rigorous model of PSA processes for gas separation is a subject very little studied in the literature. Balances of mass, energy, and moment, as well as equations on equilibrium Thermodynamic and kinetic, form a system of partial differential equations (PDE) which describe the dynamic behavior of the PSA process [8]. In most cases, there are works in the literature that make simplifications on these PDE, however, they are not feasible, since they do not have a good approximation compared to the real results, generating a loss of information and data when making these considerations. For this reason, it is necessary to use numerical methods to simulate gas flow, temperature increases and pressure drops through a packed bed for purification and production of dehydrated ethanol. Since PSA model phenomena depend on both time

The associate editor coordinating the review of this manuscript and approving it for publication was Shuihua Wang.

and space, there are two main approaches to solving the PDE equations: 1) discretizing the derivatives of time and space to obtain a model of ordinary differential equations to be solved simultaneously, or 2) perform system identification using the inputs and outputs obtained from the PSA process. [9]–[17].

Various optimization methods have been used to improve the performance of the PSA process to have an optimal and efficient process, one of these methods is machine learning technology, these methods are currently receiving a lot of attention, and they are impacting sustainable energy processes. Machine learning is an important part of artificial intelligence. There are various machine learning methods such as neural network, Bayesian linear regression, decision tree, etc [18].

In literature, a method has been reported to simulate and optimize a PSA process to separate nitrogen/air using ANN. The network they developed was used to minimize the cost objective function and it shows that it can easily be used in process optimization and/or control [19]. Subsequently, another work apply ANN to separate a N_2/CH_4 mixture in a packed bed. They analyzed using artificial neural networks (ANN) as a surrogate model to predict and optimize the PSA performance. Using the ANN surrogate model, optimization time they managed to decrease from 15.7 h to 50 s. They demonstrated that the PSA cycle proposed can achieve an optimized 99.5% nitrogen purity stream from an 85% inlet stream and a 50% purity stream from a 10% inlet stream. they also show that nitrogen recovery can be at most 90%. They further carry out a multi-objective optimization to demonstrate the tradeoff curve between nitrogen purity and recovery [20].

In more recent work, authors established an ANN model for breakthrough curves prediction about a ternary components gas with a two-layered adsorbent bed piled up with Activated Carbon (AC) and zeolite, and optimization is concluded by the ANN. The optimization is concentrated on the effect of inlet flow rate, pressure, and layer ratio of activated carbon height to zeolite height [21]. Subsequently, an investigation was developed and validated a six-step two-bed PSA model for hydrogen purification. Based on the validated PSA model, they produced a dataset to train the ANN model. the multi-objective optimization of the hydrogen purification system, they made performed based on the trained ANN model. The ANN can be considered a very effective method for predicting and optimizing the performance of the PSA system for hydrogen purification [18]. On the other hand, an integrated process for H_2 recovery and CO_2 capture from the tail gas of hydrogen plants was presented in [22]; where they propose a dynamic-model-based ANN for the integrated process was developed to optimize the performance. The synthetic datasets for the ANN were analyzed by singular value decomposition, and the ANN models for the cryogenic, membrane and PSA units were trained and tested within a marginal error ($< 2\%$).

Likewise, we found a work that was compared with published experimental results, and the yield of hydrogen purification by PSA in a stratified bed was studied numerically. Their results show that there is a contradiction between hydrogen purity and recovery, so multi-objective optimization algorithms are needed to optimize the PSA process. They used for data analysis and prediction the Machine learning methods; the polynomial regression (PNR) and ANN, they used to predict the purification performance of the two-bed six-step process [23].

NOMENCLATURE

a_p	Specific particle surface, ($m^2\ m^{-3}$)
c_i	Molar concentration of the component i, (kmol m^{-3})
D_{mi}	Molecular diffusivity i, ($m^2\ s^{-1}$)
D_{ei}	Effective phase diffusivity adsorbed from component i, ($m^2\ s^{-1}$)
C_{ps}	Specific heat capacity of adsorbent, (MJ $kmol^{-1}\ K^{-1}$)
F	Flowrate, (kmol h^{-1})
E_{zi}	Axial dispersion coefficient of component i, ($m^2\ s^{-1}$)
C_{pai}	Specific heat capacity of the adsorbed phase, (MJ $kg^{-1}\ K^{-1}$)
H_s	Heat transfer coefficient of liquid / solid, ((J s^{-1}) $m^{-2}\ K^{-1}$)
h	Element size
i	Component index
J_i	Mass transfer rate, (kmol m^{-3}(bed) s^{-1})
j	j^{th} collocation point
K	Langmuir isotherm equilibrium constant (1 Pa^{-1})
k	Iteration index
M	Molar weight, (kg mol^{-1})
l	Element index
$IP_{1i}, IP_{2i}, IP_{3i}, IP_{4i}$	Isothermal parameters of component i
MTC_s	Mass transfer coefficient solid, (1 s^{-1})
k_{sa}	Axial effective thermal conductivity (W $m^{-1}\ K^{-1}$)
P	Pressure (Pa)
Q	Isosteric heat of adsorption (J mol^{-1})
W_i	Adsorbed amount of the component i, (kmol kg^{-1})
W_i^*	Adsorbed equilibrium amount of component i, (kmol kg^{-1})
R	Universal gas constant (J $mol^{-1}\ K^{-1}$)
r_p	Adsorbent particle radius (m)
t	Time (s)
T_g	Gas temperature, (K)

T_s Solid temperature, (K)
T Temperature, (K)
u Position in element
v_g Surface gas velocity, (m s^{-1})
x Position in catalyst
y_i Molar fraction of the gas component i
z Coordinate of axial distance, (m)

No works have been developed on the PSA process for bioethanol purification using Machine Learnings, the few found are on hydrogen and nitrogen purification. One of these works implements a PSA cycle model that is simulated on the Aspen Adsorption platform and is applied to observe the dynamic behavior of a ternary-component gas mixture with a molar fraction of $H_2/CO_2/CO = 0.68/0.27/0.05$ on $Cu-BTC$ adsorbent bed. Then, they built an ANN model for predicting PSA system performance and further optimizing the operation parameters of the PSA cycle. The performance data they got from the Aspen model, they used to train the ANN model. This research shows that it is feasible to find optimal operation parameters of the PSA cycle by the optimization algorithm based on the ANN model which was trained on the data produced from the Aspen model [24]. In the same period of time, some researchers carried out the development of a 4 bed and 8 steps PSA process to produce high-purity hydrogen from the steam methane reforming gas mixture. They investigated two surrogate models to optimize the process performance using ANN, which have been well trained by the samples, obtaining from the detailed models using Latin hypercube sampling strategy. The results they obtained indicate that ANNs can approximate the performance and dynamic behavior of the PSA process with extremely high accuracy. Herein, they also proposed a robust and fast multi-objective optimization approach of the PSA process using the genetic algorithms on the support of different ANN-based surrogate models have, in which Dual- and Tri-objective optimizations are taken into account. This research that they developed shows that the method can not only find out the optimal operating conditions of the PSA process for hydrogen production with higher than 99% accuracy, namely Pareto-Optimal Fronts but also provide a reliable reference for operational enhancement [25].

II. PSA PROCESS MODEL

The ethanol purity simulations were carried out from the Aspen Adsorption program. The model that was approached for this research was taken from the work carried out by [8]. The parameters taken from this work were adapted to the equations handled by the Aspen Adsorption program, as well as the valve opening and closing configurations in the 4 steps: Adsorption, depressurization, purge, and repressurization. The following assumptions were made to achieve the expected results in the aspen adsorption program:

1) There are no reactions: There are no reactions between the elements of the mixture (water-ethanol).
2) Only one adsorbing component (water).
3) Gas mixture is assumed to be ideal.
4) Gaseous phase is convective with an estimated axial dispersion.
5) The enthalpy of the adsorbed phase is significant and it is estimated assuming constant heat capacities.
6) The axial thermal conduction for the solid phase is characterized by a constant parameter, but the radial contribution is not quantified.
7) The kinetic model is represented with Lumped Resistance Model, in the linear form, and the driving force is based on a solid (zeolite), considering the constant mass transfer coefficient.
8) The adsorption equilibrium is modeled by the Langmuir model, expressed in terms of temperature-dependent parameters.

The nature of the process and its operating conditions determine the type of model to use.

In this work, a model is presented adsorption column uses a set of PDE to represent the momentum, heat, and material balances across the column.

From the assumptions mentioned above, a summary of the equations is made for mass/Momentum and energy balances, thermodynamic and kinetic equilibrium used for the PSA process.

- Mass Balance for Gas Phase

$$-\epsilon_i E_{zi}\frac{\partial^2 c_i}{\partial z^2}+\frac{\partial(c_i v_g)}{\partial z}+\epsilon_i\frac{\partial c_i}{\partial t}+J_i=0 \tag{1}$$

where the flow over the solid surface is defined by:

$$J=-\rho\frac{\partial W_i}{\partial t} \tag{2}$$

The convection $(\frac{\partial(C_i V_g)}{\partial z})$ with estimated dispersion $(-\epsilon_i E_{zi}\frac{\partial^2 c_i}{\partial z^2})$ option assumes that the dispersion coefficient varies along the length of the bed.

- Gas Phase Energy Balance

$$-k_{sa}\frac{\partial^2 T_s}{\partial^2 z^2}+C_{ps}\rho_s+\rho_s\frac{\partial T_s}{\partial t}\sum_{i=1}^{n}(C_{pai}W_i)\frac{\partial T_s}{\partial t}+\rho_s\sum_{i}^{n}(\Delta H_i\frac{\partial W_i}{\partial t})-MTC_{ap}(T_g-T_s)=0 \tag{3}$$

The energy balance (solid phase) represents the Heat of adsorption $(\rho_s\sum_i^n(\Delta H_i\frac{\partial W_i}{\partial t}))$, accumulation of heat $(C_{ps}\rho_s+\rho_s\frac{\partial T_s}{\partial t})$, gas-solid heat transfer $(MTC_{ap}(T_g-T_s))$.

- Momentum Balance

$$-\frac{\partial P}{\partial z}=-(\frac{150x10^{-3}(1-\epsilon_i)^2}{(2r_p\Psi)^2\epsilon_i^2}\mu v_g+1.75x10^{-5}M\rho_g\frac{(1-\epsilon_i)}{2r_p\Psi\epsilon_i^3}v_g^2) \tag{4}$$

We use the Ergun equation, which combines the description of pressure drops by the Karman-Kozeny equation

$(-\frac{\partial P}{\partial z} = -(\frac{150x10^{-3}(1-\epsilon_i)^2}{(2r_p\Psi)^2\epsilon_i^2}\mu v_g)$ for laminar flow and the Burke-Plummer equation $(1.75x10^{-5}M\rho_g\frac{(1-\epsilon_i)}{2r_p\Psi\epsilon_i^3}v_g^2)$ for turbulent flow.

- Mass Transfer Rate

$$\frac{\partial W_i}{\partial t} = MTC_{si}(W_i^* - W_i) \tag{5}$$

where:

$$MTC_{si} = \frac{\Omega D_{ei}}{r_p^2} \tag{6}$$

and Ω is the parameter in the Glueckauf expression

- Langmuir Equation

$$W_i^* = \frac{IP_1 e^{ip_2/T_s}P_i}{1 + IP_3 e^{ip_4/t_s}P_i} \tag{7}$$

To solve the PDEs that represent the PSA model, initial and boundary conditions are necessary. These allow a solution and be the start-up conditions in each step (adsorption, depressurization, purge and repressurization) of the PSA process. The conditions for the first cycle in the two beds are showed in Table 2.

A. DESCRIPTION OF PSA PROCESS

The general design of the process and the operating conditions were defined considering as reference the process reported by [8].

To dehydrate ethanol, the use of type 3A zeolites was considered, they are spheres of 1 to 2 mm. This adsorbent can withstand the adsorption of water up to 22% of its own weight, has a greater attraction on water molecules, has high regeneration capacity, supports high temperatures and low pressures, provides a very large surface area compared to other zeolites (synthetic).

The process consists of two columns (beds) packed with type 3A zeolite, these columns operate in 2 stages (adsorption/regeneration) that involve 4 steps: adsorption (stage I), depressurization, purge and repressurization (stage II).

Each step is carried out at an appropriate time to meet the corresponding operational objective. Figure 1 shows the PSA process flow diagram and indicates the times of each step for each packed column. Likewise, the flow diagram includes 10 valves that serve to change the direction of the flow and maintain the flows at the desired values through the beds.

In [7] work, the steps, structure, and characteristics of the PSA process can be known in detail, as well as the values of the openings of the valves and flows.

The working pressure is 379.212 kPa, since it was observed that the higher the pressure the zeolites attract the water molecules more, and the pressure for the regeneration stage is 13.79 kPa, this is in order to easily break the weak bond that has formed between the adsorbent-adsorbate. On the other hand, the production temperature should be kept approximately constant and above 440 K. A flow of 512 $kmol\ h^{-1}$ is fed with a composition of 0.182 molar fraction of water (8% wt of water) and 0.818 molar fraction of ethanol (92 % wt of ethanol) close to the azeotropic point.

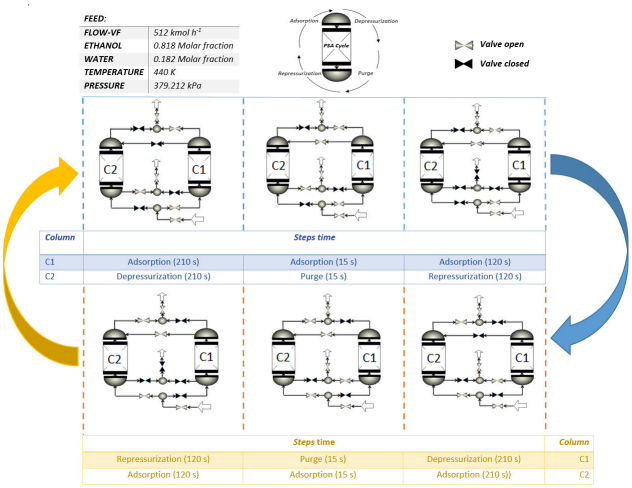

FIGURE 1. Scheme of the PSA process.

III. SIMULATION OF THE PSA PROCESS

Based on the parameters and conditions shown in Tables 1, 3 and 4, using the rigorous PSA model that is represented by Equations 1, 3, 4 and 5x, simulations are carried out in order to obtain the output signals that will be used to train an ANN.

The pressure cycle profiles with time reflect the change of the PSA dynamics process and the product obtained of ethanol purity, and temperature profiles with the operating conditions presented in Figure 1.

Figure 2 shows the profile of one pressure cycle with a duration of 690 s, the cycle comprises 4 steps: adsorption, depressurization, purge, and repressurization. The adsorption pressure is carried out at 379 *kPa* with a duration of 345 s, then depressurization is carried out reaching a value close to 50 *kPa* with a duration of 210 s, later the purge is carried out with a vacuum pressure of 18 *kPa* with a duration of 15 s and to end the repressurization is carried out in a time of 120 s,

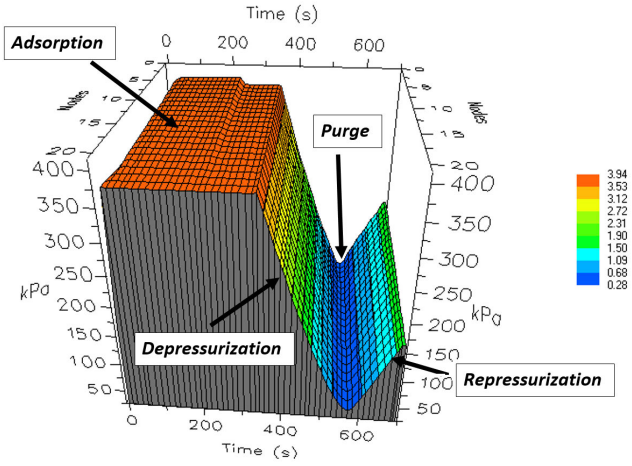

FIGURE 2. Pressure profile of a cycle.

in order to leave the bed ready to start the adsorption step again.

Figure 3 shows the 350 cycles in 69.4 h of the pressure profile and the CSS (cyclic stable state) of the PSA process is reached, at that point the profiles of both temperature and compositions (ethanol-water) are cyclically repeated without having variation (see Figures 6 and 7).

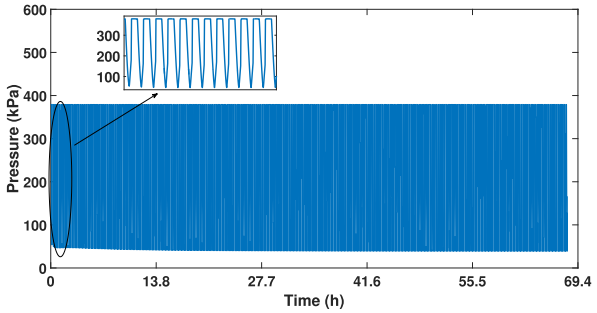

FIGURE 3. Pressure reached in the upper part of the bed from the transient start-up.

It is important to mention that due to the cyclical dynamics presented by the PSA process, the ethanol-water purity and temperature profiles tend to have oscillatory dynamics due to their cyclical nature as shown in Figures 6a and 6b.

Figures 2 and 7 present the profiles of temperature and water-ethanol concentrations during 350 PSA cycles. The bed is initially filled with a steam feed at 512 $kmol\ h^{-1}$ with a production pressure of 379 kPa and a temperature of 440 K. It can be seen that after 350 cycles (69.4 h) the profiles are stable but cyclical, resulting in a purity of 99.5% wt of ethanol (see Figure 6a). On the other hand, the water concentration decreases until reaching purities of 0.5% wt (see Figure 6b). The purity of ethanol obtained meets international standards to be used as a fuel or oxygen additive. For the temperature profile (see Figure 7), the maximum height of 7.3 m equivalent to node 20 has been chosen, it is possible to observe how in the first 20 cycles the temperature decreases, this is due to the endothermic energy that is generated between the adsorbent and the molecule of water at the time of adsorption, after 120 cycles the temperature stabilizes by a release of exothermic energy.

After having simulated the PSA process from the start-up and achieving the CSS in 350 cycles, a parametric study is carried out at the point reached (99.5% wt of ethanol) to know the primary control loop (input and output). This study is developed by adding variations generated with a uniform distribution in the possible input variables (pressure, temperature, composition, and flow) that will control the desired purity (ethanol).

A. PARAMETRIC STUDY OF THE PSA PROCESS

At this point, a parametric study was proposed to analyze the possible input variables that affect the purity obtained from the 2 bioethanol generating columns. The analysis was developed by generating steps with an increase of ±5% over

(a) Ethanol.

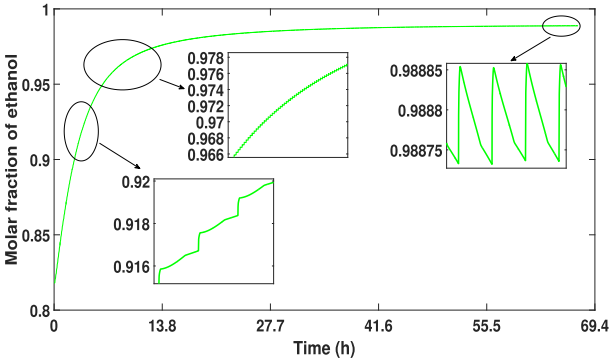

(b) Water.

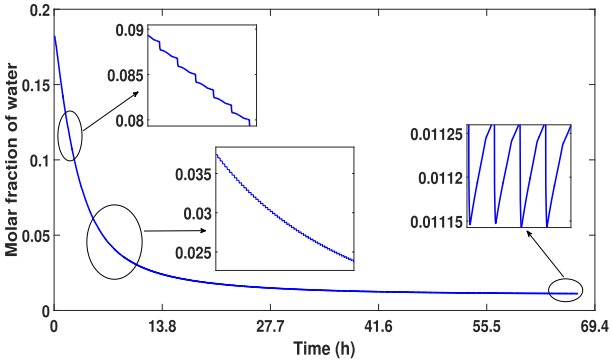

FIGURE 4. Profiles of the compositions of water-ethanol reached from the transient start-up of the bed.

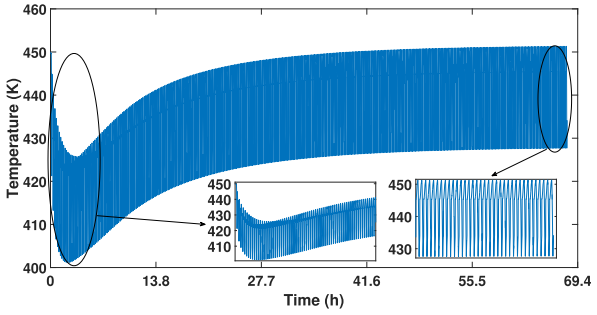

FIGURE 5. Temperature reached in the upper part of the bed from the Transient start-up.

the nominal value of the possible input variables, the results are shown in the following Figure 16.

It is possible to see the different oscillatory dynamics based on the changes generated in the inputs on the nominal value. The first case that we observe are those of the feeding temperature, these changes have a great effect on the purity obtained, giving as results purities that reach 0.9908 molar fraction (99.63 wt of ethanol) with an increase of +5% over 440 K and on the other hand, with a decrease of -5% purity of 0.9806 molar fraction (99.23% wt of ethanol) is reached. In both cases a CSS is reached again in an approximate time

(a) Purity obtained using 418 K.

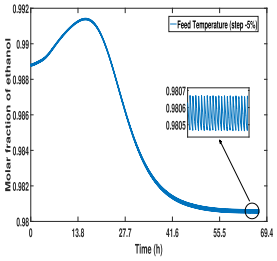

(b) Purity obtained using 462 K.

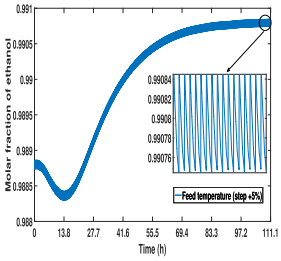

(c) Purity obtained using 486 $kg\ h^{-1}$.

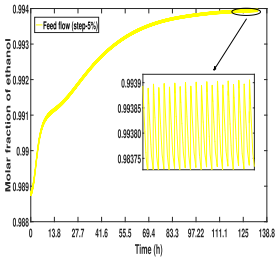

(d) Purity obtained using 537 $kg\ h^{-1}$.

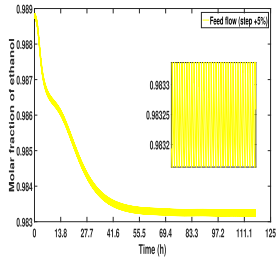

(e) Purity obtained using 360 kPa.

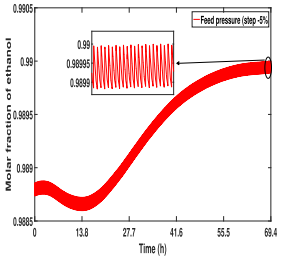

(f) Purity obtained using 398 kPa.

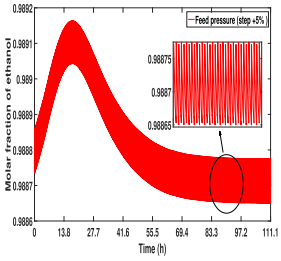

(g) Purity obtained using 0.2229 water and 0.818 ethanol.

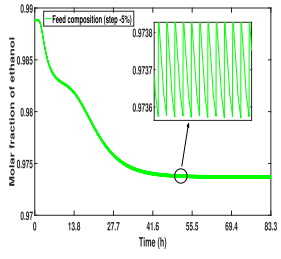

(h) purity obtained using 0.1411 water and 0.8589 ethanol.

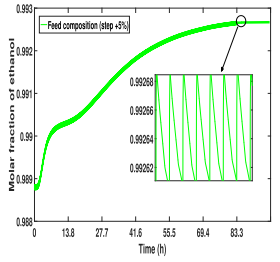

FIGURE 6. Profiles of the compositions of water-ethanol reached from the transient start-up of the bed.

of 111 h, equivalent to 579 cycles using the increase of +5% and with the decrease the CSS was reached again in 69.4 h, equivalent to 363 cycles. In summary, Table 5 shows the data obtained with the aforementioned analysis of the variations in the feeding temperature.

Table 5 shows 9 simulations, the first simulation (pink text) presents the case with nominal start-up values of the

TABLE 1. Analysis of the possible input variables that have the greatest effect on the purity obtained.

Run	Temperatura (K)	Flow $kg\ h^{-1}$	Pressure kPa	Composition Water-Ethanol	Purity % wt of ethanol	Number of cycles
1	440	512	379	0.182-0.818	99.5	350
2	418	512	379	0.182-0.818	99.23	363
3	462	512	379	0.182-0.818	99.63	579
4	440	486	379	0.182-0.818	99.75	579
5	440	537	379	0.182-0.818	99.33	370
6	440	512	360	0.182-0.818	99.60	362
7	440	512	398	0.182-0.818	99.54	440
8	440	512	379	0.2229-0.818	98.95	327
9	440	512	379	0.1411-0.8589	99.71	464

PSA process, a purity of 99.5% is obtained, which meets international standards to be used as a fuel or additive oxygenating. Based on the nominal start-up values and being in the CSS, changes of ±5% were made on the variables of temperature (blue text), flow (yellow text), pressure (red text), and composition (green text).

After having simulated each of the changes generated in the possible input variables (see figure 6), it was observed (see Table 5) that the effects on the purity obtained (ethanol) are favorable in different characteristics. The input variable that generated the highest purity was the effect of the feed flow with a step of -5%, this variable generates the highest purity (99.75% wt of ethanol) compared to the effects of the other input variables, however, the cycle time to achieve this purity was 579. On the other hand, the input variable that presented the greatest quickness generating an insignificant increase in purity (99.60% wt of ethanol) was the feed pressure with a cycle time of 362. For the cases of the input variables of temperature and feed composition, the results in purities obtained were below the purity obtained with the changes of the feed flow variable and concerning cycle times, these were greater compared to the cycle time generated by the feed pressure.

Therefore, the feed flow can be defined as an input variable, since it has a greater effect on the purity of ethanol obtained as the final product. It is important to mention that although it takes more time to reach CSS, what is sought is to have more control in achieving a large increase in the purity obtained.

After having defined the input and output variable, the identification of the PSA process will be carried out with these two signals, generating an excitation on the rigorous PSA model, to obtain a model in ANN that capture the important dynamics of the process PSA.

IV. SYSTEM IDENTIFICATION

A. SYSTEM DESCRIPTION

The rigorous PSA model presented in the previous section acts as a virtual PSA plant, with the objective of evaluating its dynamic performance under various operating conditions and achieving acquisition input and output data, which are used to identify a reduced or simplified model capable of capturing the important dynamics of the PSA process. The importance of system identification is based on finding a reduced model

(a) Input signals (feed flow).

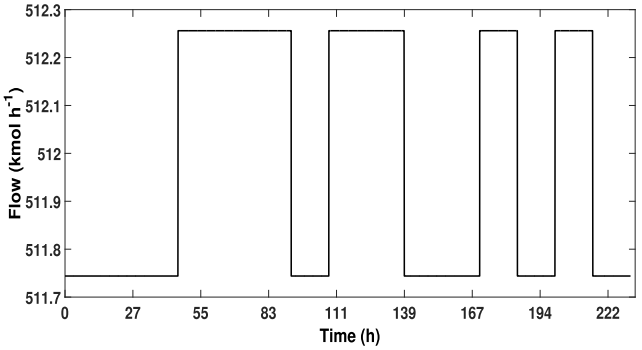

(b) Output signals (ethanol purity).

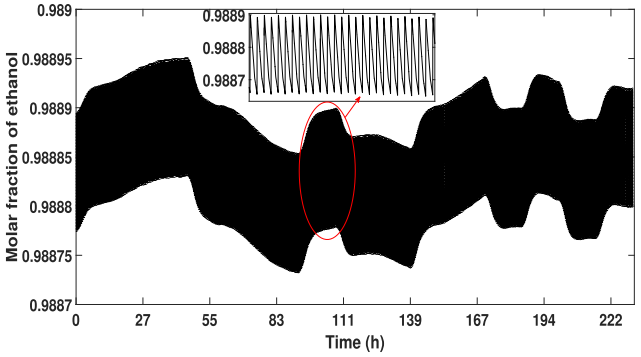

FIGURE 7. Ethanol purity response to feeding flow pulses with different time amplitudes.

that relates the input variable (feed flow) and the output variable (ethanol purity) with a good approximation to the rigorous PSA model.

In this work, input data (Figure 19a) were generated from the nominal value of the feed flow. The development of the array of inputs was from the design of a 5 bits PRBS with a variation of $\pm 0.5\%$ that includes a time for the purity of ethanol to converge in a CSS, this is shown in the time from 0 to 49 h. These data were injected into the rigorous PSA model resulting in output data (Figure 19b), these variations of signals that are injected into the rigorous PSA model persistently excite the system, obtaining variations in the purity of ethanol and comply with the aim of obtaining a reduced and less complex model.

The input and output data are shown in the Figure 19a and 19b. These signals are used in order to identify the reduced model. As is mentioned above, this data is defined as the inlet steam with a composition of 0.183 water and 0.818 of ethanol in molar fraction and, the output is the bioethanol purity. The database is composed by 799200 samples, each sample is taken every second. The dataset was divided in two different parts to estimate and validate the models that is, 399600 samples to estimate the parameters of the model and 399600 unknown samples to validate the model.

B. PROPOSED SYSTEM MODELING

Figure 8 shows the Artificial Neural-Network (ANN) architecture used in this paper. The ANN is composed of three layers in order to process the inputs of the ANN which are the input and output of the real system. This input layer which is composed of two neurons, splits the input and output completely in order to generalize the auto regressive models, that is, if the activation functions were identity functions ($f(x) = x$), the ANN structure would be an autoregressive model with exogenous input. Then, the ANN is composed of a hidden layer with two neurons in order to add more degrees of freedom. Finally, in the output layer, the proposed ANN is composed of one neuron which it is in charge for linking the dynamics of the input and output of the system. The ANN is composed of five neurons in total. One of the neurons at the input layer processes the input monitored signals and propagates its resulting output vector v_u to an independent hidden neuron. The other input neuron processes the previous n_a outputs of the ANN, and propagates its output vector v_y to a second independent hidden network. Finally, both hidden neurons feed the output neuron to produce the estimated bioethanol purity $\hat{y}[k]$. this is the reason of the ANN name. Therefore, the neural model represented in Figure nn1 is described by 8.

$$
\begin{aligned}
&haty[k] \\
&= X\varphi_3(z_{\hat{y}}\varphi_2\left(v_{\hat{y}}\varphi_1\left(\sum_{i=1}^{n_a} w_{\hat{y}}^{i}\hat{y}[k-i]+\theta_{\hat{y}}\right)+v_{\hat{y}h}\right) \\
&+ z_u\varphi_2\left(v_u\varphi_1\left(\sum_{j=1}^{n_b} w_u^{j}u[k-n_k-j]+\theta_u\right)+v_{uh}\right)+z_h)
\end{aligned}
\tag{8}
$$

where X, $z_{\hat{y}}$, $v_{\hat{y}}$, $\theta_{\hat{y}}$, $v_{\hat{y}h}$, z_u, v_u, θ_u, v_{uh}, $z_h \in \mathbb{R}$, $w_{\hat{y}} \in \mathbb{R}^{n_a}$, and $w_u \in \mathbb{R}^{n_b}$ represents the parameter of the model or the well known synaptic weights. Finally, the model output and inputs dynamics is represented for $\hat{y}[k]$ and $u[k]$ respectively.

For this research paper, the synaptic weights are computed with a learning algorithm based on gradient descendent such

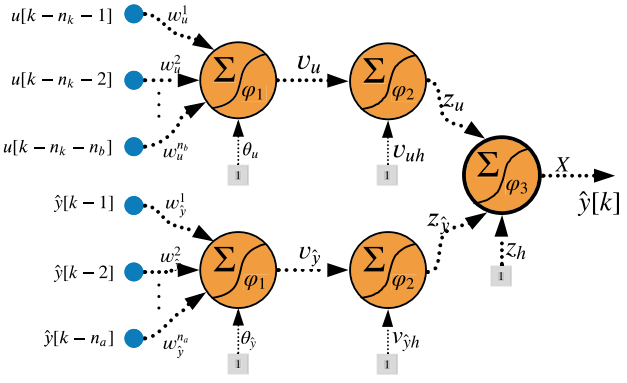

FIGURE 8. 2-2-1 Neural-Network for system identification.

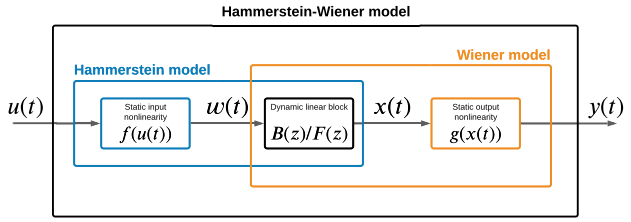

FIGURE 9. Structure of the hammerstein-wiener model.

as the Levenberg-Marquardt algorithm shown in Eq. (9),

$$\Delta W_k = \left[J(W_k)^T J(W_k) + \mu I\right]^{-1} J(W_k) e^T, \tag{9}$$

where W_k represents the parameter to optimize, $J(\cdot)$ represents the Jacaobian matrix based in the parameter W_k, μ the learning rate and e represents the difference between the real output and the output obtained by the ANN.

As is shown in Eq. (8), there are several parameters to estimate in spite of the synaptic weights, these parameters are the regression values which allows to represent the system dynamics. Otherwise (the case where the system is static), these parameters does not exist. The parameters n_a, n_b and n_k are chosen with the implementation of a grid search algorithm, that is, an interval composed of integer positive numbers is proposed for each parameter for instance, $n_a = \{1, 2, 3, \cdots, NA\}$, $n_b = \{1, 2, 3, \cdots, NB\}$, $n_k = \{1, 2, 3, \cdots, NK\}$. The values of NA, NB and NK are chosen by the user. In this sense, the grid search algorithm realize and evaluate the performance of each possible combination from these n_a, n_b and n_k parameters. The result of the process is an array with $NA \times NB \times NK$ possible performance combinations.

This methodology has been proposed in several research papers in order to develop the system identification procedure of vast and different systems. The effectiveness of this ANN structure is presented in the following papers [26]–[30].

V. RESULTS

A Hammerstein-Wiener (HW) model has been also proposed in order to compare the performance of our model with another identification techniques. The HW model is a series connection of a static nonlinear blocks with a dynamic linear block. This kind of methodology is suitable to use it in different areas such as electromechanical systems modeling, radio frequency components, audio, speech processing, predictive control, etc. [31]–[33]. The identified HW model is also implemented in [17] and, its structure is shown in Fig. 22.

According to the Fig. nn1 description and, selecting as $\varphi_2(x) = \varphi_3(x) = x$ and $\varphi_1(x) = \tanh(x)$ then, the ANN equation is expressed as Eq. (10).

$$\hat{y}[k] = V_{\hat{y}} \tanh\left(\sum_{i=1}^{n_a} w_{\hat{y}}^i \hat{y}[k-i] + \theta_{\hat{y}}\right) + V_u \tanh\left(\sum_{i=1}^{n_b} w_u^i u[k-n_k-i] + \theta_u\right) + V_h \tag{10}$$

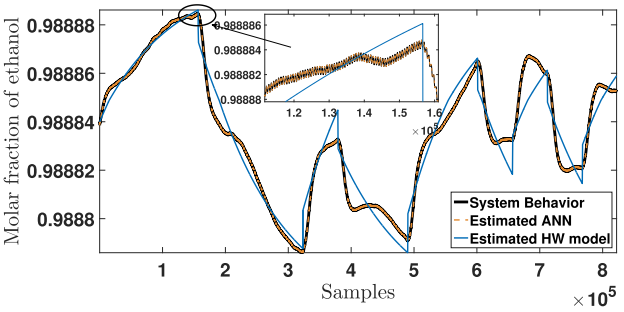

FIGURE 10. Temporal behavior of the real system, HW model and ANN model.

In order to optimize the regression parameters (n_a, n_b and n_k), the FIT shown in Eq. (11)

$$FIT = 100 * \left(1 - \frac{||y - \hat{y}||}{||y - \bar{y}||}\right) \tag{11}$$

where y represents the real output of the system, $\hat{y}$ represents the simulated output from the identified model and $\bar{y}$ represents the mean of the real output signal. The root mean square error was also used as shown in Eq. (12) with the same proposes.

$$RMSE = \sqrt{\frac{\sum_{i=1}^{N}(x_i - \hat{x}_i)^2}{N}}, \tag{12}$$

where, x_i represents a sample of the real output system and, $\hat{x}_i$ is a sample of the estimated output system.

The result of this procedure is the selection of $n_a = 8$, $n_b = 6$ and $n_k = 4$. Therefore, the total number of model parameters is 19. Figure r1 shows the behavior of both models with the same input, this figure is shown in order to illustrate how the models acts according to real input signal. The FIT equation (see Eq. (11)) shows how a signal is related with another, i.e., if the estimated output is strongly similar to the real system output, the computed FIT would be close to 100%. In this sense, the HW model has obtained a 75.8325% while, the ANN model has obtained a 97.9985%.

A comparison of the distribution of each system is included, in the Figures 11 and 12, the distribution of each estimation is shown where, the ANN model is superior than the HW model due, the distribution of the real system and the ANN model is almost the same. In order to compare numerically these relations, the RMSE (shown in Eq. (12)) is computed. The RMSE value shows the mean distance between two signals using the error (which is a comparison between the real and estimated signal and is shown in Eq. (13)), i.e., if both signal are similar then the RMSE tends to zero otherwise, the error can tend to infinity. In this sense, the RMSE computed for the HW model is 6.4175**e**-06 while the ANN model has obtained 1.4490**e**-09 which is more than

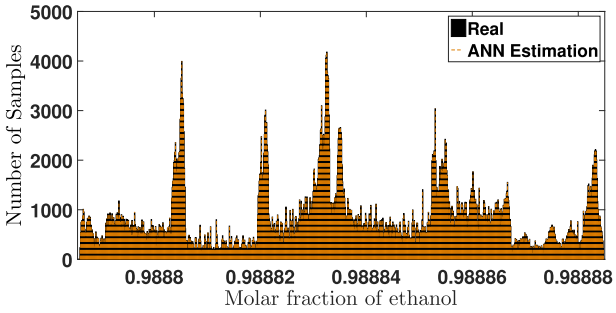

FIGURE 11. Distribution of the real output system and the output generated by the ANN model.

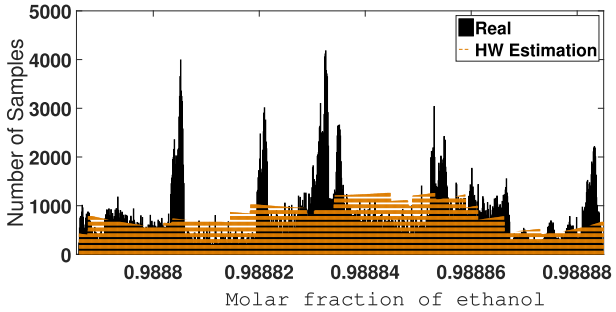

FIGURE 12. Distribution of the real output system and the output generated by the HW model.

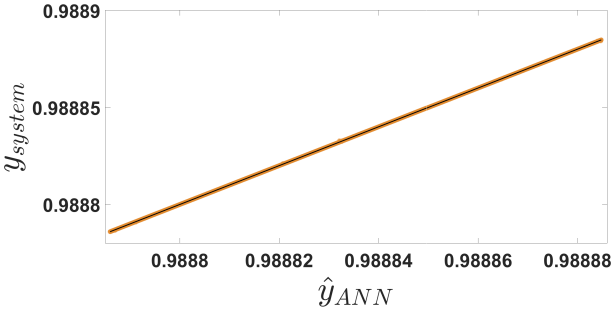

FIGURE 13. Slope-intercept test for the ANN model.

one thousand times the RMSE provided by the HW model.

$$e := y - \hat{y}, \tag{13}$$

where y represents the real output signal and $\hat{y}$ is the estimated output.

Finally, the slope-intercept test is performed in order to include another statistical test to our estimated system. Ideally, the slope should be equal to one and the intercept equal to zero in the representation of a strength line which fits to the comparison between the real output signal and the estimated signal.

In this case, the slope of the ANN is $m = 1$ and intercept $b = 0$. While, the slope computed for the HW model is $m = 0.9992$ and intercept $b = 0.0008$ which is acceptable and competitive with the ANN model.

The results obtained from the modeling by means of an artificial neural network were highly satisfactory in all the tested senses. The results have been compared with other

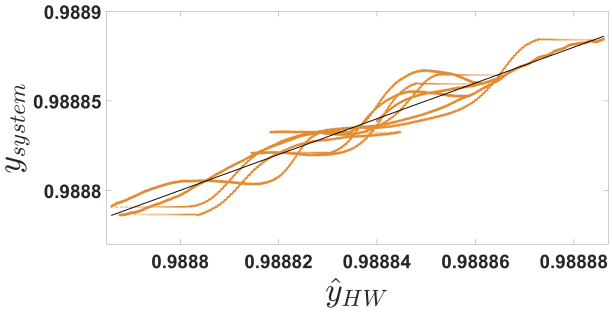

FIGURE 14. Slope-intercept test for the HW model.

systems identification techniques such as the Hammerstein-Winner model, which is a highly used method for the identification of real plants. Even with this comparison, the neural network model was highly satisfactory.

VI. CONCLUSION

The system identification procedure is an empirical modeling method in order to obtain or propose a model that mimics the real behavior of a real system. In this method, the real system output and input signals are the only information needed in order to compute the model. As is shown above, there exist several methodologies in order to identify a system, in this research, an ANN is proposed which, has been compared with an HW model. The ANN has shown the best performance among the computed models (HW vs ANN), using several testing procedures and performance indexes, for instance, the FIT where the ANN has a 97.9985% while the HW model has 75.8325%. In the particular case of the slope-intercept test, the performance of both models is similar due to the system output amplitude; which has not any major changes through time, i.e., the output oscillations are between 0.998879 and 0.98888. In the same sense, the RMSE in both methods are similar because the difference of the real output and estimated output are close to the amplitude of the oscillations, even if this error is small, the ANN has shown a better performance than the HW model. On the other hand, if the number of parameters is compared, the ANN model estimates its output with 19 parameters to represent the real system behavior while, the HW model requires around 37 parameters to estimate the output real system; this is not a substantial difference on the implement ion point of view but, it is for the models quality, the quality of a model is related strongly by the number of estimated parameters, in this sense, when the model has a low number of parameters, the quality is high. Therefore, with 19 parameters the ANN model quality is higher than the HW model. Finally, we can conclude that it is of great importance to obtain a model identified with ANN to design controllers, since in the highly non-linear rigorous PSA model it is difficult to design controllers. Another contribution of this new model identified with ANN, allows a better approximation to the ethanol purity results that can be obtained in the real PSA plant, therefore this new model can be used to predict the dynamic behavior and avoid a decrease

in ethanol purity, allowing the real plant to have predictions to adjust its parameters and avoid these loss problems.

COMPETING INTERESTS

The authors declare that they do not have any competing interests on this manuscript.

APPENDIX A

TABLE 2. Initial and boundary conditions.

Adsorption (Cycle step I):	Purgue (Cycle step III):
t = 0; $y = W = 0, T = T_f, P = P_f$	t = 0; $y = y^{(II)}, W = W^{(II)}, T = T^{(II)}, P = P^{(II)}$
z = 0; $y = y_f, T = T_f, F = F_f$	z = 0; $y = y_p, T = T_p, F = F(valve)$
z = L; $\frac{\partial y}{\partial z} = 0, \frac{\partial T}{\partial z} = 0$	z = L; $P = P_p, \frac{\partial y}{\partial z} = 0, \frac{\partial T}{\partial z} = 0$
Depressurization (Cycle step II):	Represurization (Cycle step IV):
t = 0; $y = y^{(I)}, W = W^{(I)}, T = T^{(I)}, P = P^{(I)}$	t = 0; $y = y^{(III)}, W = W^{(III)}, T = T^{(III)}, P = P^{(III)}$
z = 0; $\frac{\partial y}{\partial z} = 0, \frac{\partial T}{\partial z} = 0$	z = 0; $y = y_p, T = T_p, F = F(valve)$
z = L; $\frac{\partial y}{\partial z} = 0, \frac{\partial T}{\partial z} = 0, F = F(Valve)$	z = L; $\frac{\partial y}{\partial z} = 0, \frac{\partial T}{\partial z} = 0$

APPENDIX B

TABLE 3. Operating parameters of the PSA process [8] and [17].

	Value	Units
Bed height	7.3	m
Internal diameter of bed	2.4	m
Inter-particle voidage	0.4	m^3 void m^{-3}
Intra-particle voidage	0.63	m^3 void m^{-3}
Adsorbent shape factor	1	n/a
Constant mass transfer coefficient (Ethanol)	1.996	s^{-1}
Constant mass transfer coefficient (Water)	2.949	s^{-1}
Molecular diffusivity (ethanol)	$2.1796e^{-5}$	$m^2 s^{-1}$
Molecular diffusivity (Water)	$3.728e^{-6}$	$m^2 s^{-1}$
Heat Capacity of the adsorbent	1260	$JKg^{-1}K^{-1}$
Constant for heat of adsorption (Water)	-39.3	MJ $kmol^{-1}$
Constant for heat of adsorption (Ethanol)	-51.9	MJ $kmol^{-1}$
Constant for the heat transfer coefficient	$1e^6$	J s^{-1} m^{-2} K^{-1}
Adsorbent thermal conductivity	41.26	Wm^{-1} K^{-1}

TABLE 4. PSA process feed parameters.

	Value	Units
Production temperature	440	K
Production pressure	379.212	kPa
Purge Pressure	13.79	kPa
Molar fraction (Water)	0.182	kmol $kmol^{-1}$
Molar fraction (Ethanol)	0.818	kmol $kmol^{-1}$
Number of nodes	20	
Discretization Method	OCFE2	

TABLE 5. Characteristics of the adsorbent and parameters of the Langmuir isotherm [8] and [17].

	Value	Units
Bulk density of adsorbent	729.62	kg m^{-3}
Adsorbent particle radius	0.0015875	m
$IP1$ (Water)	$1.9064e^{-7}$	Pa^{-1}
$IP2$ (Water)	6242.13	Pa^{-1}
$IP3$ (Water)	$1.7874e^{-5}$	Pa^{-1}
$IP4$ (Water)	6242.13	Pa^{-1}
$IP_{1,2,3,4}$ (Ethanol)	0	Pa^{-1}
Specific surface area of adsorbent	1133.86	m^{-1}

REFERENCES

[1] S. Kumar, N. Singh, and R. Prasad, "Anhydrous ethanol: A renewable source of energy," *Renew. Sustain. Energy Rev.*, vol. 14, no. 7, pp. 1830–1844, Sep. 2010.

[2] C. Cantero, G. Lopez, V. Alvarado, R. Jimenez, J. Morales, and E. Coronado, "Control structures evaluation for a salt extractive distillation pilot plant: Application to bio-ethanol dehydration," *Energies*, vol. 10, no. 9, p. 1276, Aug. 2017.

[3] V. Pasa, *Recomendaciones de Especificaciones Técnicas Para el Etanol y Sus Mezclas (E-6), y la Infraestructura Para su Manejo en México*. Mexico City, Mexico: SENER/GTZ, 2010, p. 100. [Online]. Available: http://www.gtz.de/

[4] ASTM International. (2009). *ASTM D4806–09 Standard Specification for Denatured Fuel Ethanol for Blending with Gasolines for Use as Automotive Spark-Ignition Engine Fuel*. [Online]. Available: https://www.astm.org/DATABASE.CART/HISTORICAL/D4806-09.htm

[5] ASTM International. (2020). *ASTM D5798–20 Standard Specification for Ethanol Fuel Blends for Flexible-Fuel Automotive Spark-Ignition Engines*. [Online]. Available: https://www.astm.org/Standards/D5798.htm

[6] J. Y. Rumbo-Morales, G. Lopez-Lopez, V. M. Alvarado, J. S. Valdez-Martinez, F. D. Sorcia-Vázquez, and J. A. Brizuela-Mendoza, "Simulation and control of a pressure swing adsorption process to dehydrate ethanol," *Revista Mexicana Ingeniería Química*, vol. 17, no. 3, pp. 1051–1081, Jul. 2018. [Online]. Available: http://www.rmiq.org/ojs311/index.php/rmiq/article/view/123

[7] J. Y. R. Morales, J. A. B. Mendoza, G. O. Torres, F. D. J. S. Vázquez, A. C. Rojas, and A. F. P. Vidal, "Fault-tolerant control implemented to Hammerstein–Wiener model: Application to bio-ethanol dehydration," *Fuel*, vol. 308, Jan. 2022, Art. no. 121836.

[8] M. Simo, C. J. Brown, and V. Hlavacek, "Simulation of pressure swing adsorption in fuel ethanol production process," *Comput. Chem. Eng.*, vol. 32, no. 7, pp. 1635–1649, Jul. 2008.

[9] Y. Liu, J. Delgado, and J. A. Ritter, "Comparison of finite difference techniques for simulating pressure swing adsorption," *Adsorption*, vol. 4, no. 3, pp. 337–344, 1998, doi: 10.1023/A:1008898019954.

[10] J. Guan and X. Hu, "Simulation and analysis of pressure swing adsorption: Ethanol drying process by the electrical analogue," *Separat. Purification Technol.*, vol. 31, no. 1, pp. 31–35, 2003.

[11] M. Bitzer, "Model-based nonlinear tracking control of pressure swing adsorption plants," in *Control and Observer Design for Nonlinear Finite and Infinite Dimensional Systems* (Lecture Notes in Control and Information Science), vol. 322, Nov. 2005, pp. 403–418, doi: 10.1007/11529798_25.

[12] M. A. Latifi, D. Salhi, and D. Tondeur, "Optimisation-based simulation of a pressure swing adsorption process," *Adsorption*, vol. 14, nos. 4–5, pp. 567–573, Oct. 2008.

[13] H. Khajuria and E. N. Pistikopoulos, "Dynamic modeling and explicit/multi-parametric MPC control of pressure swing adsorption systems," *J. Process Control*, vol. 21, no. 1, pp. 151–163, 2011.

[14] J. Macron, J. Pierquin, O. Roy, and P. Rouchon, "Purity predictive model-based control of oxygen vacuum swing adsorption process," in *Proc. 18th Medit. Conf. Control Automat.*, 2010, pp. 745–749.

[15] H. Peng, F. Couenne, and Y. L. Gorrec, "Robust control of a pressure swing adsorption process," *IFAC Proc. Volumes*, vol. 44, no. 1, pp. 7310–7315, Jan. 2011.

[16] H. Khajuria and E. N. Pistikopoulos, "Optimization and control of pressure swing adsorption processes under uncertainty," *AIChE J.*, vol. 59, no. 1, pp. 120–131, 2013, doi: 10.1002/aic.13783.

[17] J. Y. R. Morales, G. L. López, V. M. A. Martínez, F. D. J. S. Vázquez, J. A. B. Mendoza, and M. M. García, "Parametric study and control of a pressure swing adsorption process to separate the water–ethanol mixture under disturbances," *Separat. Purification Technol.*, vol. 236, Apr. 2020, Art. no. 116214.

[18] L. Tong, P. Bénard, Y. Zong, R. Chahine, K. Liu, and J. Xiao, "Artificial neural network based optimization of a six-step two-bed pressure swing adsorption system for hydrogen purification," *Energy AI*, vol. 5, Sep. 2021, Art. no. 100075.

[19] J. Lewandowski, N. O. Lemcoff, and S. Palosaari, "Use of neural networks in the simulation and optimization of pressure swing adsorption processes," *Chem. Eng. Technol.*, vol. 21, no. 7, pp. 593–597, Jul. 1998. [Online]. Available: https://www.researchgate.net/publication/230175717_Use_of_Neural_Networks_in_the_Simulation_and_Optimization_o_Pressure

[20] H. R. Sant Anna, A. G. Barreto, F. W. Tavares, and M. B. de Souza, "Machine learning model and optimization of a PSA unit for methane-nitrogen separation," *Comput. Chem. Eng.*, vol. 104, pp. 377–391, Sep. 2017.

[21] S. Ma, L. Tong, F. Ye, J. Xiao, P. Bénard, and R. Chahine, "Hydrogen purification layered bed optimization based on artificial neural network prediction of breakthrough curves," *Int. J. Hydrogen Energy*, vol. 44, no. 11, pp. 5324–5333, Feb. 2019.
[22] N. D. Vo, D. H. Oh, J.-H. Kang, M. Oh, and C.-H. Lee, "Dynamic-model-based artificial neural network for H_2 recovery and CO_2 capture from hydrogen tail gas," *Appl. Energy*, vol. 273, Sep. 2020, Art. no. 115263. [Online]. Available: https://yonsei.pure.elsevier.com/en/publications/dynamic-model-based-artificial-neural-network-for-hsub2sub-recove
[23] J. Xiao, C. Li, L. Fang, P. Böwer, M. Wark, P. Bénard, and R. Chahine, "Machine learning–based optimization for hydrogen purification performance of layered bed pressure swing adsorption," *Int. J. Energy Res.*, vol. 44, no. 6, pp. 4475–4492, May 2020, doi: 10.1002/er.5225.
[24] F. Ye, S. Ma, L. Tong, J. Xiao, P. Bénard, and R. Chahine, "Artificial neural network based optimization for hydrogen purification performance of pressure swing adsorption," *Int. J. Hydrogen Energy*, vol. 44, no. 11, pp. 5334–5344, Feb. 2019.
[25] X. Yu, Y. Shen, Z. Guan, D. Zhang, Z. Tang, and W. Li, "Multi-objective optimization of ANN-based PSA model for hydrogen purification from steam-methane reforming gas," *Int. J. Hydrogen Energy*, vol. 46, no. 21, pp. 11740–11755, Mar. 2021.
[26] H. M. Romero Ugalde, J.-C. Carmona, J. Reyes-Reyes, V. M. Alvarado, and C. Corbier, "Balanced simplicity–accuracy neural network model families for system identification," *Neural Comput. Appl.*, vol. 26, no. 1, pp. 171–186, Jan. 2015.
[27] H. M. Romero Ugalde, J.-C. Carmona, J. Reyes-Reyes, V. M. Alvarado, and J. Mantilla, "Computational cost improvement of neural network models in black box nonlinear system identification," *Neurocomputing*, vol. 166, pp. 96–108, Oct. 2015.
[28] H. M. Romero Ugalde, J.-C. Carmona, V. M. Alvarado, and J. Reyes-Reyes, "Neural network design and model reduction approach for black box nonlinear system identification with reduced number of parameters," *Neurocomputing*, vol. 101, pp. 170–180, Feb. 2013.
[29] C. J. Zúñiga-Aguilar, J. F. Gómez-Aguilar, H. M. Romero-Ugalde, H. Jahanshahi, and F. E. Alsaadi, "Fractal-fractional neuro-adaptive method for system identification," *Eng. Comput.*, pp. 1–24, Feb. 2021.
[30] C. J. Zuñiga Aguilar, J. F. Gómez-Aguilar, V. M. Alvarado-Martínez, and H. M. Romero-Ugalde, "Fractional order neural networks for system identification," *Chaos, Solitons Fractals*, vol. 130, Jan. 2020, Art. no. 109444.
[31] A. Brouri, F.-Z. Chaoui, and F. Giri, "Identification of Hammerstein–Wiener models with hysteresis front nonlinearities," *Int. J. Control*, pp. 1–15, Sep. 2021.
[32] Q. Nguyen, S. A. Bagherzadeh, A. Parsian, M. Akbari, A. Karimipour, and A. Mosavi, "Nonlinear model identification of dissimilar laser joining of S.S 304 and ABS using the Hammerstein–Wiener method," *Optik*, vol. 225, Jan. 2021, Art. no. 165649.
[33] A. Wills, T. Schön, L. Ljung, and B. Ninness, "Identification of Hammerstein–Wiener models," *Automatica*, vol. 49, no. 1, pp. 70–81, Jan. 2013.

ERASMO MISAEL RENTERÍA-VARGAS received the bachelor's degree in electronic engineering from the Higher Technological Institute of Zapopan, Zapopan, Mexico, and the master's degree in project management from the Technological University of Mexico, Mexico. He is currently pursuing the Ph.D. degree in physical-mathematical sciences with Los Valles University Center, with a focus on digital signal processing. He is currently a Professor of subject "A" with the University Center of the Valleys, University of Guadalajara (UdeG). One of the projects carried out is the construction and automation of a pilot plant to obtain bioethanol through the PSA process using neural networks to identify purity. His main research interests include process techniques for biofuels and neural network design.

CARLOS JESÚS ZÚÑIGA AGUILAR received the Ph.D. degree in electronics from the Centro Nacional de Invistigacion y Desarrollo Tecnologico (CENIDET), with a focus on automatic control. He has worked in several national and international projects in Mexico and France, where he has developed machine learning models in order to predict diseases and glucose levels. Currently, he is working as a Data Scientist with Panzura. His research interests include automatic control, system identification, financial models, machine learning, and deep learning.

JESSE YOE RUMBO MORALES (Member, IEEE) received the Ph.D. degree from the Centro Nacional de Investigacion y Desarrollo Tecnologico (CENIDET). He is currently a full time Professor with the University of Guadalajara. He has published national and international journal articles with cites from Scopus. He has graduated 15 bachelor's degree thesis and 15 technical level theses. He has participated in projects, in particular in the construction of a prototype PSA to produce bioethanol. Belongs to the SNI. His research interests include process control, renewable energy, identification of non-linear systems, and automation.

FELIPE DE JESÚS SORCIA VÁZQUEZ was born in Orizaba, Mexico, in 1985. He received the B.S. degree in electronics engineering from the Instituto Tecnologico de Orizaba, Orizaba, in 2008, and the M.Sc. degree in electronics engineering and the Dr.Sc. degree from the Centro Nacional de Investigacion y Desarrollo Tecnologico (CENIDET), Cuernavaca, Mexico, in 2010 and 2015, respectively. He is currently a Professor and a Researcher with the University of Guadalajara. He is a member of the National Research System (SNI), Mexico. His research interests include model predictive control, distributed and decentralized model predictive control, nonlinear control, and real-time control applications.

MIGUEL DE-LA-TORRE (Senior Member, IEEE) received the Ph.D. degree from the École de Technologie Superieure, in 2015. Since 2006, he has been a full-time Teacher and a Researcher with the Department of Computer Science and Engineering, University of Guadalajara. As a member of the Computer Science Academy, he collaborates in graduate and undergraduate engineering programs with the University Center of Los Valles. Since 2017, he has been a Distinguished National Researcher with the National System of Researchers, Mexico. His research interests include adaptive pattern recognition, signal, and image processing applied to biometrics, scene analysis and understanding, food engineering, and satellite imagery.

JOSÉ ANTONIO CERVANTES received the B.S. degree in computational systems from the Instituto Tecnologico de Jiquilpan, Mexico, in 2003, and the M.S. degree in computer science from the Centro Nacional de Investigacion y Desarrollo Tecnologico (CENIDET), Mexico, in 2005, and the Ph.D. degree in electronic engineering from the Centro de Investigacion y de Estudios Avanzados del IPN (CINVESTAV), Mexico, in 2015. Since 2017, he has been an Associate Professor with the Computational Sciences and Engineering Department, Universidad de Guadalajara. His research interests include artificial vision on UAVs, brain-inspired cognitive architectures for artificial intelligence, and social robots for therapeutic purposes.

ESTELA SARMIENTO BUSTOS was born in Morelos, Mexico, in 1966. She received the B.S. degree in chemical industrial engineering from the Instituto Tecnologico de Zacatepec, Morelos, and the M.S. and Ph.D. degrees in engineering and applied sciences from the Universidad Autonoma del Estado de Morelos, Morelos. She is currently a full time Professor with the Universidad Tecnologica Emiliano Zapata del Estado de Morelos, Morelos. Her main research interests include corrosion and thin film deposition techniques and characterization.

MANUELA CALIXTO RODRÍGUEZ was born in Zacatecas, Mexico, in 1975. She received the degree in communication and electronic engineering from the Universidad Autonoma de Zacatecas, Zacatecas, and the M.S. and Ph.D. degrees in renewable energy from the Universidad Nacional Autonoma de Mexico, Mexico. She is currently a full-time Professor with the Universidad Tecnologica Emiliano Zapata del Estado de Morelos, Morelos, Mexico. Her main research interests include semiconductor thin film deposition techniques and characterization and instrumentation on research.